arXiv:1405.4313v4 [cond-mat.str-el] 17 Jun 2015

Mixed configuration ground state in Iron(II) Phthalocyanine

Javier Fernández-Rodríguez,[1,2] Brian Toby,[2] and Michel van Veenendaal[1,2]

[1]*Department of Physics, Northern Illinois University, DeKalb, Illinois 60115, USA*
[2]*Advanced Photon Source, Argonne National Laboratory, 9700 South Cass Avenue, Argonne, Illinois 60439, USA*

(Dated: June 18, 2015)

We calculate the angular dependence of the x-ray linear and circular dichroism at the $L_{2,3}$ edges of α-Fe(II) Phthalocyanine (FePc) thin films using a ligand field model with full configuration interaction. We find the best agreement with the experimental spectra for a mixed ground state of ${}^3E_g(a_{1g}^2e_g^3b_{2g}^1)$ and ${}^3B_{2g}(a_{1g}^1e_g^4b_{2g}^1)$ with the two configurations coupled by the spin-orbit interaction. The ${}^3E_g(b)$ and ${}^3B_{2g}$ states have an easy axis and plane anisotropies, respectively. Our model accounts for an easy-plane magnetic anisotropy and the measured magnitudes of the in-plane orbital and spin moments. The proximity in energy of the two configurations allows a switching of the magnetic anisotropy from easy plane to easy axis with a small change in the crystal field, as recently observed for FePc adsorbed on an oxidized Cu surface. We also discuss the possibility of a quintet ground state (${}^5A_{1g}$ is 250 meV above the ground state) with planar anisotropy by manipulation of the Fe-C bond length by depositing the complex on a substrate that is subjected to a mechanical strain.

I. INTRODUCTION

Metal phthalocyanines (MPc's) have many technological applications in catalysis [1], photodynamic cancer therapy [2] and, given their semiconducting properties, in solar cells [3]. Another field of potential interest of MPc's is their use as magnetic materials [4, 5], with applications as magnetic storage devices, quantum computing, and molecular spintronics [6, 7]. Understanding the microscopic interactions that govern their magnetic properties is of key importance in the design of functional materials. In addition to the magnetic interactions (exchange) amongst the building blocks, magnetic anisotropy has an important role in the magnetic properties of a material. In planar MPc's the metal center is surrounded by the four pyrrolic nitrogens of the macrocycle in an environment of D_{4h} symmetry. The d-orbitals of the metal-center are split into the four representations of the group [8]: $a_{1g}(d_{z^2})$, $b_{1g}(d_{x^2-y^2})$, e_g (d_{zx}, d_{yz}), and $b_{2g}(d_{xy})$. Ligand-field models [9] can give the energy levels of the individual orbitals and provide an adequate formalism for describing the ground state and magnetic anisotropy of the individual single molecule magnets [10].

Fe(II)-Phthalocyanine (FePc) is a promising candidate for its use as a magnetic material given its strong magnetic anisotropy. The tunability of the magnetization axis has been the subject of recent study [11, 12] for its possible application in spintronics. Despite having been a subject of study for several decades, the ground state configuration of FePc is still a matter of debate since it was originally proposed [13, 14] as ${}^3E_g(a_{1g}^1e_g^3b_{2g}^2)$ (in the following we abbreviate this ground state labeling as ${}^3E_g(a)$, see footnote [50]). Several density functional theory studies give different predictions. Liao and Scheiner get a ${}^3A_{2g}(a_{1g}^2e_g^2b_{2g}^2)$ ground state [15]. ${}^3A_{2g}$ has also been proposed based on x-ray measurements. [16] Marom *et al.* get ${}^3B_{2g}(a_{1g}^1e_g^4b_{2g}^1)$ or ${}^3A_{2g}$ depending on computational details [17]. Nakamura *et al.* [18] found ${}^3A_{2g}$ for isolated FePc and ${}^3E_g(a)$ for linear chains. Recently, from multiplet calculations [19, 20] the ground state was found to be ${}^3E_g(b)$. Kuzmin *et al.* [21] also found ${}^3E_g(b)$ using a superposition crystal field model [22]. The possibility of ${}^3E_g(b)$ and ${}^3B_{2g}$ lying very close in energy and being mixed by spin-orbit coupling has been suggested [19, 23]. A mixed quintet-triplet ground state has also been proposed [24]. Mössbauer and x-ray dichroism measurements in thin films of α-FePc [25, 26] give valuable information about the electronic structure of FePc, demonstrating that the complex has planar magnetic anisotropy, i.e., it is easier to magnetize the molecule parallel to the plane and that the Fe ion has a large unquenched orbital moment $m_L \approx 0.5\mu_B$.

In this paper, we use the multiplet model implemented in the xclaim code [27, 28] to calculate the $L_{2,3}$ edges x-ray spectra in FePc and determine the metal center ground state configuration and crystal field energy levels. By calculating the expectation values of the orbital and spin moments we can determine the angular anisotropy and estimate the errors affecting the application of the XMCD sum rules [29, 30] in this system. From a fit of the angular dependence of the x-ray absorption measurements in thin films of α-FePc by Bartolomé *et al.* [26] we determine the values of the D_{4h} crystal-field parameters and find a ground state of mixed ${}^3E_g(b)$ and ${}^3B_{2g}$ character. We discuss the magnetic anisotropies corresponding to the single configurations ${}^3E_g(b)$ and ${}^3B_{2g}$, and propose ${}^3E_g(b)$ with easy axis anisotropy as the ground state in FePc adsorbed on an oxidized Cu surface. From exact diagonalization we calculate the crystal-field excitations. The presence of a low-lying ${}^5A_{1g}$ configuration, makes it feasible to produce a quintet ground state with planar anisotropy by manipulations of the Fe-C bond length.

TABLE I: Hartree-Fock atomic parameters for the Fe^{2+} ion in the base $3d^6$ and excited $2p^5 3d^6$ atomic configurations in units of eV. In the calculation of the spectra we apply a 70% reduction to the Slater integrals.

parameter	base config.	excited config.
$F^2(3d)$	10.966	11.779
$F^4(3d)$	6.815	7.328
$\zeta(3d)$	0.052	0.067
$F^2(2p,3d)$		6.793
$G^1(2p,3d)$		5.001
$G^3(2p,3d)$		2.844
$\zeta(2p)$		8.201

II. LIGAND-FIELD MODEL

For the Fe^{2+} ion ($3d^6$) we use a ligand-field many-body hamiltonian with full configuration-interaction taking into account the Coulomb, spin-orbit coupling, crystal field and Zeeman interactions. Hartree-Fock estimates of the radial part of matrix elements of the Coulomb interaction in terms of Slater integrals F^k and G^k and the spin-orbit coupling parameters $\zeta(3d)$ and $\zeta(2p)$ for the core $2p$ and valence $3d$ valence shells. are obtained from Cowan's atomic multiplet program RCN [31, 32]. Their values are shown in table I. The Slater integrals F^k and G^k are reduced to 70% of their Hartree-Fock values to account for the effect of hybridization.

The crystal field hamiltonian is written in terms of Wybourne parameters [33, 34] as

$$H_{\rm CF} = \sum_{k,q} B_{kq} C_q^{(k)} \tag{1}$$

with $0 \le k \le 2l$, k an even integer and $-k \le q \le k$. B_{kq} are the Wybourne parameters and $C_q^{(k)}$ are renormalized spherical harmonics $C_q^{(k)} = \sqrt{\frac{4\pi}{2k+1}} Y_q^k$. The relationship $B_{k,-q} = (-1)^q B_{kq}^*$ holds because of the hermiticity of the hamiltonian.

For a d-shell in D_{4h} symmetry, we can relate the B_{20}, B_{40} and B_{44} Wybourne parameters to the Ballhausen notation Dq, Ds and Dt [8],

$$\begin{aligned} B_{20} &= -7Ds \\ B_{40} &= 21(Dq - Dt) \\ B_{44} &= 21\sqrt{\frac{5}{14}} Dq \end{aligned} \tag{2}$$

In D_{4h} the d-orbitals are split into four representations. Their energies are, in terms of the Ballhausen parameters,

$$\begin{aligned} \epsilon_{a_{1g}} &= 6Dq - 2Ds - 6Dt \\ \epsilon_{b_{1g}} &= 6Dq + 2Ds - Dt \\ \epsilon_{b_{2g}} &= -4Dq + 2Ds - Dt \\ \epsilon_{e_g} &= -4Dq - Ds + 4Dt \end{aligned}$$

With the crystal field definition of Eq. (1) we can calculate the effect of a rotation of the local ligand environment by rotating the Wybourne parameters as a spherical tensor [35]. The crystal field resulting from a rotation with Euler angles $\alpha\beta\gamma$ is expressed by

$$B'_{kq} = \sum_{-k \le q' \le k} B_{kq'} D^K_{q'q}(\alpha\beta\gamma), \tag{3}$$

with the matrix elements $D^k_{q'q}(\alpha\beta\gamma)$ given by

$$D^k_{qq'}(\alpha\beta\gamma) = \exp(-iq\alpha) d^k_{qq'}(\beta) \exp(-iq'\gamma), \tag{4}$$

where $d^k_{qq'}(\beta)$ is a Wigner d-function. [35]. In this paper we consider a rotation of the sample about the y-axis and Equation (3) reduces to

$$B'_{kq} = \sum_{-k \le q' \le k} B_{kq'} d^k_{q'q}(\theta), \tag{5}$$

where θ denotes the incidence angle of the x-rays with respect to the c-axis. Particularizing for the case of a d-shell in D_{4h} symmetry, the rotated crystal-field parameters can be written as

$$\begin{aligned} B'_{2q} &= B_{20} d^2_{0q}(\theta) \\ B'_{4q} &= B_{40} d^4_{0q}(\theta) + B_{44}[d^4_{4q}(\theta) + d^4_{-4q}(\theta)]. \end{aligned} \tag{6}$$

III. XAS AND MAGNETIC ANISOTROPY

A. Fit to the experimental spectra

We calculate the angular dependence of the linearly polarized x-ray absorption and XMCD by rotating the crystal field parameters and maintaining both the x-ray wavevector $\mathbf{k}$ and the 5 T applied magnetic field $\mathbf{H}$ parallel to the z-direction. For the core-hole lorentzian broadenings we use the values $\Gamma_L = 0.2$ and 0.37 eV for the Fe L_3 and L_2 edges [36] and $\Gamma_{Gauss} = 0.5$ eV to account for the experimental resolution. The additional broadening observed in the experimental spectra [26] comes from the formation of electronic bands due to the columnar stacking of molecules in α-FePc.

The best fit to the experimentally measured spectra corresponds to the crystal field parameters $Dq = 0.175$, $Ds = 0.970$, $Dt = 0.150$ eV. Figure 1 shows the crystal field energy levels of the d-orbitals and the calculated XAS spectra is plotted in Fig. 2. We obtain a ground state of mixed ${}^3E_g(e_g^3 a_{1g}^2 b_{2g}^1)$ and ${}^3B_{2g}(e_g^4 a_{1g}^1 b_{2g}^1)$ character. The occupation of the orbitals in the mixed ground state is $(a_{1g}^{1.7} b_{2g}^1 e_g^{3.3})$, with part of the charge of the a_{1g} orbital being moved to the e_g (d_{zx}, d_{yz}) orbitals. When we switch off the spin-orbit interaction in our model, the mixture of the configurations disappears and ${}^3E_g(b)$ is

the ground state with ${}^3B_{2g}$ 80 meV higher in energy. Fig. 1(b) shows a level diagram with the energies of the d-d excitations. The next excitation is ${}^5A_{1g}(e_g^2 a_{1g}^2 b_{1g}^1 b_{2g}^1)$ 250 meV above the ground state [Fig. 1(b)]. There are no other excitations within approximately 1 eV. Our calculation gives a good account of the angular dependence of the lineraly polarized XAS and XMCD when comparing it with the experimental measurements [26]. The main shortcoming in our model is the absence of XMCD at $\theta = 0$ (Fig. 2(b)).

By exactly diagonalizing the Hamiltonian we can get the zero field splitting (ZFS) of the mixed configuration ground state. The excited states are 2.4, 3.6, 11, 47, 130 and 160 meV above the ground state. The states at 3.6 and 130 eV are doublets and the rest are singlets. The applied magnetic field is not producing a reordering of the zero-field energy levels, since their splittings are greater than the energy changes induced by the magnetic field, in the order of ($\mu_B H \approx 0.3$ meV).

In addition to the x-ray spectra, we look at the magnetic anisotropy of the Fe ion. In Fig. 2(c) we show the expectation values of the orbital $\langle m_L \rangle_\theta$ and spin $\langle m_S \rangle_\theta = 2\langle S \rangle_\theta$ magnetic moment components along the magnetic field as a function of θ. We calculate both the expectation value of the spin moment, and the spin effective $\langle m_S^{\rm eff} \rangle_\theta$, that is obtained by applying the spin sum rule [30] to the calculated XMCD. Several factors contribute to the discrepancy between the expectation value of the spin moment and its sum rule value: the magnetic dipolar term $\langle T \rangle$ [37, 38], and the mixing of spectral weight between the L_2 and L_3 edges occurring in early transition metals [39, 40]. Another source of error is the fact that for practical applications of the sum rule the isotropic intensity is approximated as the average of left and right circularly polarized absorption [41] $I_{iso} = I_z + I_+ + I_- \approx 3/2(I_+ + I_-)$. An experimental measurement of the intensity with linear polarization along the z-axis I_z would require the x-ray beam to be in the transverse direction. At 5 T applied field, we get the moments in the ab-plane (see Fig. 2(c) at $\theta = 90^o$) $\langle m_L^{ab} \rangle = 0.5\mu_B$, and $\langle m_S^{{\rm eff},ab} \rangle = 0.7\mu_B$ in good agreement with the experimental values obtained by XMCD measurements [26].

B. Single configurations ground-states

In addition to the mixed configuration ground state that gives the best fit, we also show the spectra corresponding to individual configuration ground states ${}^3E_g(b)$ and ${}^3B_{2g}$. In our crystal field model, we can control the mixing in the ground state of the two configurations by changing the energy positioning of the d_{z^2} orbital with respect to the other d-orbitals (see Eq. 3), and obtain single configuration ground states ${}^3E_g(b)$ or ${}^3B_{2g}$. In terms of Ballhausen parameters this corresponds to maintaining Dq constant and using the new parameters $Ds' = Ds - \Delta\epsilon_{z^2}/7$ $Dt' = Dt - \frac{3}{35}\Delta\epsilon_{z^2}$, with $\Delta\epsilon_{z^2}$ the change in energy of the d_{z^2} orbital. For ${}^3E_g(b)$ we use $Ds = 1.0275$, $Dt = 0.1845$ eV [Fig. 3(a)-(c)] and for ${}^3B_{2g}$, $Ds = 0.913$, $Dt = 0.116$ eV [Fig. 3(d)-(f)].

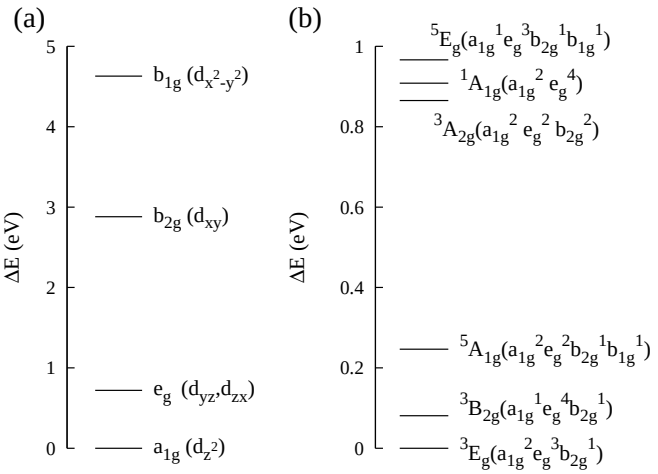

FIG. 1: (a) Crystal field levels of the d-orbitals in FePc obtained from the fitting of the experimental spectra [26] and (b) energy level diagram showing the ground state and lowest-lying *dd* excitations obtained from exact diagonalization of the many-body hamiltonian.

The two single configuration ground states would have different magnetic anisotropies. For ${}^3E_g(b)$ would be easy-axis with no magnetic moment in the plane [Fig. 3(c)] and for ${}^3B_{2g}$ would be easy-plane [Fig. 3(f)]. A simple explanation for this behavior is given by the formalism for the magnetic anisotropy developed within a perturbative treatment of spin-orbit interaction. [37, 42, 43]. Considering only spin-preserving excitations, the anisotropy energy is proportional to the orbital moment, and we can discuss the anisotropy by looking at the occupations of the single-particle orbitals in the ground state. [37]. For ${}^3B_{2g}$ d_{xy} and d_{z^2} are singly occupied. d_{z^2} cannot generate orbital moment along the c-axis, and d_{xy} can only generate orbital moment along the c-axis from excitations to $d_{x^2-y^2}$, which is much higher in energy (2 eV). In ${}^3B_{2g}$ the orbital moment in the ab-plane comes from from $e_g \longrightarrow a_{1g}$ ($d_{zx}, d_{yz} \longrightarrow d_{z^2}$) and $e_g \longrightarrow b_{2g}$ ($d_{zx}, d_{yz} \longrightarrow d_{xy}$) excitations. The case of ${}^3E_g(b)$ is different; since there is one hole in the e_g orbitals with $m_l = \pm 1$, orbital moment along the c-axis can be generated and the anisotropy is easy-axis.

C. XAS angular dependence

To understand the linearly polarized XAS spectral features in terms of transitions to valence orbitals we calculate the angular dependence of the cross-section of dipolar transitions with the incidence angles to different orbitals in the final state in terms of a single particle model. A similar discussion for the isotropic and XMCD spectra

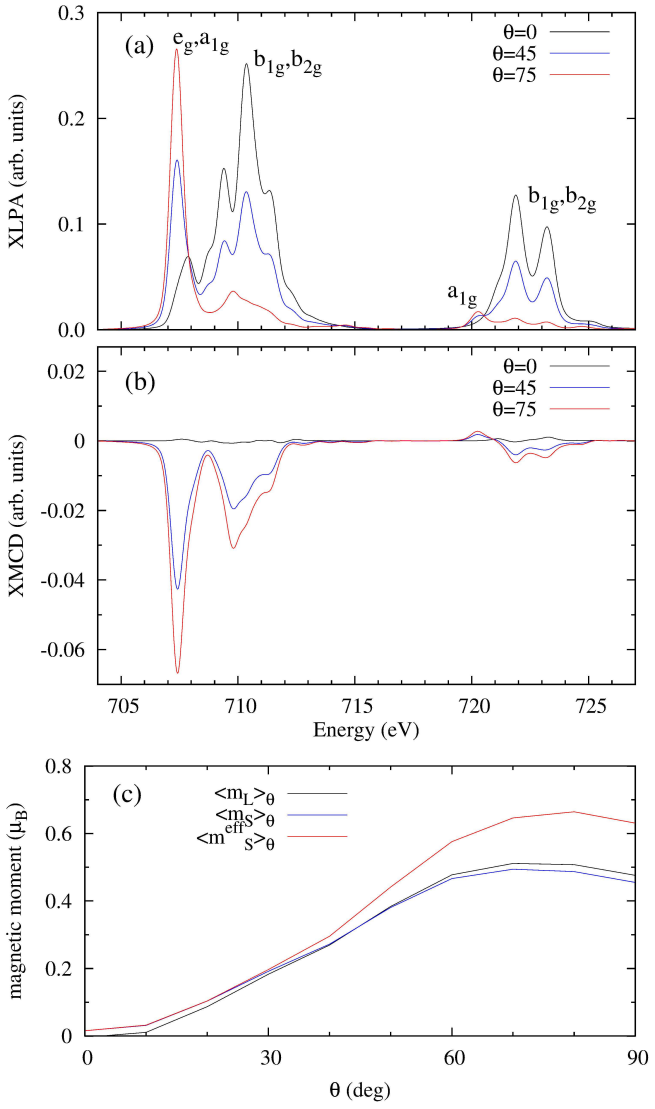

FIG. 2: Best fit to the experimental x-ray linearly polarized absorption (XLPA) (a) and XMCD (b) at the Fe $L_{2,3}$ edges. We show the calculated spectra for different x-ray incidence angles $\theta = 0, 45, 75^o$ with respect to the FePc C_4 axis. The XLPA plot (a) includes the classification of the absorption peaks in terms of transitions to valence orbitals belonging to different representations of D_{4h}. The spectra correspond to a mixed ${}^3E_g(b)$ and ${}^3B_{2g}$ ground state. We also show in (c) the expectation values of the spin $\langle m_S\rangle_\theta$ and orbital $\langle m_L\rangle_\theta$ magnetic moments along the direction of the applied magnetic field (H=5 T) as a function of θ. We also include the effective spin moment $\langle m_S^{\rm eff}\rangle_\theta$ that results from applying the spin sum-rule to the calculated spectra.

can be seen in Ref. 44. For a representation Γ of the point group D_{4h} the absorption of linearly polarized x-rays is

$$I_\Gamma(\theta) = \sum_{m_j,\gamma} |\langle 3d,\gamma|D(\theta)|2p,jm_j\rangle|^2 \qquad (7)$$

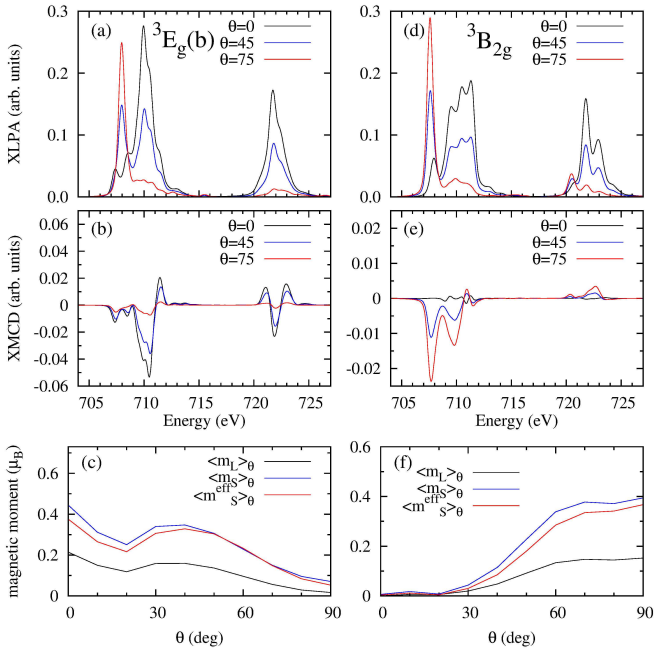

FIG. 3: Dependence with the x-ray incidence angle θ of the x-ray linearly polarized absorption (XLPA) and XMCD for single-configuration ${}^3E_g(b)$ (a),(b) and ${}^3B_{2g}$ (d),(e) ground states. (c),(f) Angular dependence of the expectation values of the spin $\langle m_S\rangle_\theta$ and orbital $\langle m_L\rangle_\theta$ magnetic moments along the magnetic field together with the spin magnetic moment determined from the XMCD sum rule $\langle m_S^{\rm eff}\rangle_\theta$.

where γ label the d-shell orbitals belonging to the Γ representation and m_j label the p-shell core states with $j = 3/2,\ 1/2$ for the L_3, L_2 edges. $D(\theta)$ is the dipolar operator corresponding to linear polarization in the xz-plane forming an angle θ with the x-axis:

$$D(\theta) = \cos\theta\frac{1}{\sqrt{2}}(D_{-1} - D_{+1}) + i\sin\theta D_0 \qquad (8)$$

the component D_q ($q = 0, \pm 1$) of the dipolar operator in spherical coordinates are

$$D_q = \sqrt{2}\sum_{m,m',\sigma}(-1)^m \begin{pmatrix} 2 & 1 & 1 \\ -m & q & m' \end{pmatrix} d^\dagger_{m,\sigma}p_{m',\sigma}. \qquad (9)$$

The resulting angular dependencies for linear polarization are given in table II. The relative intensities for the different representations are the same for the L_3 and L_2 edges.

In Fig. 2(a) we label the features of the XAS spectra according to transitions to valence orbitals belonging to different representations of D_{4h}. The sharp feature at the beginning of the L_3 edge (707 eV) increases its intensity with θ and appears for both the ${}^3B_{2g}$ and ${}^3E_g(b)$ ground states. We assign it to transitions to the d_{z^2} or to the e_g (d_{zx}, d_{yz}) orbitals contributing to the absorption at the same x-ray energy. The transition at 720 eV

TABLE II: Angular dependence of the linearly polarized x-ray absorption for single particle orbitals belonging to the different representations Γ of D_{4h} as a function of the x-ray incidence angle θ.

Γ	d-orbitals	$I(\theta)$
a_{1g}	d_{z^2}	$\frac{2}{45}(1+3\sin^2\theta)$
b_{1g}	$d_{x^2-y^2}$	$\frac{2}{15}\cos^2\theta$
b_{2g}	d_{xy}	$\frac{2}{15}\cos^2\theta$
e_g	d_{yz}, d_{zx}	$\frac{1}{15}(1+\sin^2\theta)$

at the low energy side of the L_2 edge visible in the linear polarization absorption at $\theta = 75^o$ can be assigned to transitions to the d_{z^2} orbital, given its appearance at high θ and the fact that it increases in intensity when the number of holes in d_{z^2} increases. For a pure $^3E_g(b)$ ground state [Fig. 3(a)], there are no holes in d_{z^2} and the 720 eV peak does not appear. The tails of the L_2 and L_3 edges decrease at higher θ. We assign them to transitions to $b_{2g}(d_{xy})$ and $b_{1g}(d_{x^2-y^2})$ orbitals. Both of them have the same angular dependence decreasing at higher incidence angle θ.

IV. GROUND STATE CHANGES AND MAGNETIC ANISOTROPY SWITCHING

Recently, the anisotropy of FePc has been reported to change from easy plane to easy axis when adsorbed on an oxidized Cu(110) surface [11]. Tsukahara *et al.* [11] interpret the zero field splitting for isolated FePc in terms of a simple model with an orbitally non-degenerate ground state in which the zero-field splitting would only have two levels [13] and attribute the observation of a more complex zero field splitting, and an easy-axis magnetic anisotropy of FePc adsorbed on an oxidized Cu(110) surface to the breaking of D_{4h} symmetry. However, a $^3E_g(b)$ configuration, with orbital degeration, can account for a complex zero field splitting and an easy-axis magnetic anisotropy.

In Fig. 4 we show the changes in the ground state and magnetic anisotropy as a function of the perturbations of the crystal-field potential. The modifications of the a_{1g} and b_{1g} single-particle orbital energies can be related to different physical effects: the a_{1g} potential can be changed by axial ligand coordination [45], or when the complex is adsorbed in a surface [11, 12]. The b_{1g} energy would be modified by changes in the Fe-C bond length. By changing $\varepsilon(a_{1g})$ [Fig. 4(a-d)] the ground state changes between $^3E_g(b)$ and $^3B_{2g}$ and the anisotropy changes between easy-plane and easy-axis. A reduction in $\varepsilon(a_{1g})$ as small as 0.1 eV is enough to change the magnetic anisotropy to easy-axis. The maximum of the in-plane generated moment corresponds to the region of mixed ground state, and decreases when increasing $\varepsilon(a_{1g})$ [Fig. 4(b)]. This can be easily understood, since the increase in $\varepsilon(a_{1g})$ diminishes the orbital moment generated by $e_g \longrightarrow a_{1g}$ excitations. It is worth noting that the mixed-configuration ground-state exists within a region of about 0.4 eV in the crystal field energies, where the a_{1g} orbital has a non-integer occupation [Fig. 4(c)].

Changing the energy of the b_{1g} orbital [Fig. 4(e-h)] will produce a change in spin from triplet to a quintet $^5A_{1g}$ with planar anisotropy. Reducing $\varepsilon(b_{1g})$ by 0.2 eV will start populating the b_{1g} orbital [Fig. 4(g)]. Reductions beyond 0.3 eV produce a pure quintet ground state and saturate the in-plane magnetic moment [Fig. 4(f)]. Within a small intermediate region where $^5A_{1g}$ is mixed with ^3E_g magnetic moment can be generated along the FePc axis [Fig. 4(e)]. The changes in the energy of b_{1g} can be related to changes in the Fe-C bond-length in FePc. By considering the a_{1g} crystal-field energy unaffected by the bond-length change, we can consider the energy difference between a_{1g} and b_{1g} ($\approx$ 5 eV) proportional to r^{-5} [46]. An increase of 1% in the Fe-C bond-length ($\Delta r \approx 0.02$ Å) would produce a quintet ground state. This kind of spin transition produced by increasing in-plane bond-lengths is feasible by depositing the complex on a substrate (graphene, polymers, etc.) and exerting a mechanical strain on the substrate [47].

V. CONCLUSIONS

We have used a ligand field model with full configuration interaction to calculate the magnetic properties and $L_{2,3}$ XAS spectra of FePc. Our multiplet model gives a good account of the shape and angular dependence of the experimental x-ray linearly polarized absorption and XMCD spectra measured in thin films of α-FePc. The best fit to the experimental spectra corresponds to the D_{4h} crystal field parameters $Dq = 0.175$, $Ds = 0.970$, $Dt = 0.150$ eV. This corresponds a ground state of mixed $^3E_g(b)$ and $^3B_{2g}$ character, as originally suggested by Reynolds *et al.* [23]. The two configurations are separated by a small amount of energy ($\approx$ 80 meV) and the spin-orbit interaction produces a mixed ground state. Although $^3E_g(b)$ (easy axis) is lower in energy, the mixing induced by the spin-orbit produces a ground state with easy plane anisotropy. The use of a full configuration interaction formalism makes possible to describe accurately the magnetic properties of the system in the mixed configuration.

FePc is an excellent candidate for applications in spintronics and information storage, with several ground states with different magnetic properties accessible by small changes in the ligand environment of the Fe ion. The close proximity in energy of two configurations with different easy magnetization axes makes it easy to manipulate the magnetic anisotropy with very small changes in the crystal field. The $^3E_g(b)$ configuration, with easy axis anisotropy, would be a plausible ground state for FePc adsorbed on an oxidized Cu surface, where a change of the magnetization axis has been reported. [11] In ad-

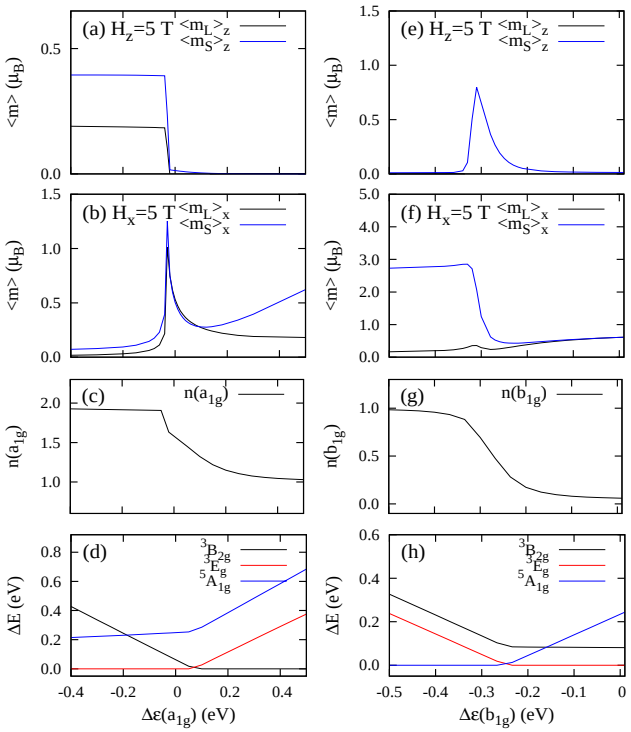

FIG. 4: Changes in the ground state and magnetic anisotropy as a function of the change in the crystal-field energies: (a-d) varying the energy of the a_{1g} (d_{z^2}) orbital and (e-h) changing the b_{1g} ($d_{x^2-y^2}$) energy. $\Delta\varepsilon(a_{1g})$ and $\Delta\varepsilon(b_{1g})$ correspond to the difference in the single-particle orbital energies from the fitted values. The plots show the orbital and spin magnetic moments generated for axial and in-plane applied fields, the changes in the orbital occupations and the energies relative to the ground state for the three configurations $^3B_{2g}$, $^3E_g(b)$ and $^5A_{1g}$. The splitting of the configurations produced by spin-orbit coupling are not shown in (d) and (h).

dition, the presence of a low-lying $^5A_{1g}$ configuration 250 meV above the ground state, makes feasible to produce a quintet ground state with planar anisotropy by expansions of the Fe-C bond length in the order of 0.02 Å. This can be achieved by depositing the complex in a substrate that is subjected to a mechanical strength.

The formalism used in this paper for the analysis of the XAS angular dependence can be applied to study other systems and get information about the ground state and *dd* excitations. The presence of low lying crystal-field excitations close to the ground state can identify candidate systems for technological applications with tunable magnetic properties where changes in the ligand environment would be able to change the ground state.

VI. ACKNOWLEDGMENTS

We thank F. Bartolomé for initially pointing us to the XAS measurements in FePc. We acknowledge useful discussions with D. Haskel, U. Staub and J.A. Blanco. This work was supported by the U. S. Department of Energy (DOE), Office of Basic Energy Sciences, Division of Materials Sciences and Engineering under Award No. DE-FG02-03ER46097, the time-dependent x-ray spectroscopy collaboration as part of the Computational Materials Science Network (CMSCN) under grant DE-FG02-08ER46540, and NIU Institute for Nanoscience, Engineering, and Technology. Work at Argonne National Laboratory was supported by the U. S. DOE, Office of Science, Office of Basic Energy Sciences, under contract No. DE-AC02-06CH11357. This work utilized computational resources at NERSC, supported by the U.S. DOE Contract No. DE-AC02-05CH11231.

Appendix A: Sum rule applicability for Fe^{2+}

In this appendix we test the validity of the spin sum rule for Fe^{2+} ($3d^6$). The estimations of the sum rule error are useful for estimating the reliability of XMCD magnetization measurements of Fe^{2+} ions. A particular case of interest is $SrFeO_2$ [48, 49], where the changes in coordination leads to physical properties that are not well understood. We take several ground states as test cases and apply the sum rule to calculated XMCD spectra and compare the sum rule derived values with the ground state expectation of the spin.

We take into account triplet and quintet ground states in tetragonal, octahedral and trigonal symmetries. It is worth noting that for $Fe^{(II)}$ in octahedral symmetry it is not possible to obtain a triplet ground state [20]. Since the sum rule actually measures the expectation value of the effective spin $\langle SE_z\rangle = \langle S_z + \frac{7}{2}T_z\rangle$ which includes the magnetic dipole term T_z, we plot the expectation values of both spin S_z and spin effective SE_z moments.

Fig. 5 shows the spin magnetic moment $\langle m_S\rangle_\theta$ along the direction of the applied magnetic field (H=5 T) for several ground states in D_{4h}, O_h and D_{3h} point groups. The spin moment is shown together with the effective spin $\langle m_{SE}\rangle_\theta$ that includes the magnetic dipole contribution and the spin moment $\langle m_{SR}\rangle_\theta$ determined from applying the sum rule to the calculated XMCD spectra. The values used for the crystal field parameters can be seen in the supplemental material addendum.

The two contributions to the sum rule error: (the magnetic dipole term T_z and the mixing of the L_2 and L_3 edges) can be seen clearly in the plots. The plots show a very good agreement of the sum rule with the expectation value of the spin moment for triplet ground states with relative errors of less than 20% as can be seen in Fig. 5(a), (b) and (e). However for quintet ground states (Fig. 5 c,d and f) the relative error is much bigger and in the case of $^5A_{1g}$ in D_{4h} symmetry (Fig. 5c) the spin

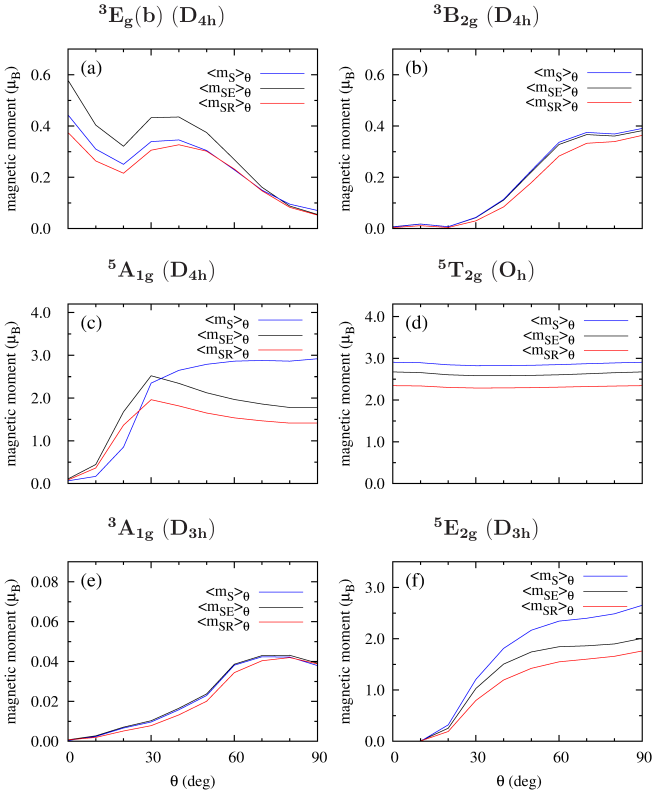

FIG. 5: Spin magnetic moment $\langle m_S\rangle_\theta$ along the direction of the applied magnetic field (H=5 T) as a function of the rotation angle θ of the ligand environment for different ground states in tetragonal (D_{4h}), octahedral (O_h) and trigonal (D_{3h}) symmetries. The spin moment values are plotted together with the effective spin $\langle m_{SE}\rangle_\theta$ that includes the magnetic dipole contribution ($SE_z = S_z + \frac{7}{2}T_z$) and the spin value $\langle m_{SR}\rangle_\theta$ determined from the application of the spin sum rule to the calculated XMCD spectra.

moment is twice of the value measured by the sum rule.

[1] C. C. Leznoff and A. B. P. Lever, *Phthalocyanines, Properties and Applications* (1996).
[2] E. Reddi, G. Lo Castro, R. Biolo, and G. Jori, Br. J. Cancer **56**, 597 (1987).
[3] K. Kadish, K. Simth, and R. Guillard, *Applications of Phthalocianines, The Porphyrin Handbook* (2003).
[4] H. Miyoshi, H. Ohya-Nishiguchi, and Y. Deguchi, Bull. Chem. Soc. Jpn. **46**, 2724 (1973).
[5] W. Kirner, J. F.and Dow and R. Scheidt, Inorg. Chem. **15**, 1685 (1976).
[6] L. Bognani and W. Wernsdorfer, Nature Mater. **7**, 179 (2008).
[7] S. Sanvito, J. Mater. Chem. **17**, 4455 (2007).
[8] C. J. Ballhausen, *Introduction to Ligand Field Theory* (1962).
[9] M. W. Haverkort, M. Zwierzycki, and O. K. Andersen, Phys. Rev. B **85**, 165113 (2012).
[10] D. Gatteschi and L. Sorace, Journal of Solid State Chemistry **159**, 253261 (2001).
[11] N. Tsukahara, K.-i. Noto, M. Ohara, S. Shiraki, N. Takagi, Y. Takata, J. Miyawaki, M. Taguchi, A. Chainani, S. Shin, et al., Phys. Rev. Lett. **102**, 167203 (2009).
[12] J. Hu and R. Wu, Physical Review Letters **110**, 097202 (2013).
[13] B. W. Dale, R. J. P. Williams, C. E. Johnson, and T. L. Thorp, Journal of Chemical Physics **49**, 3441 (1968).
[14] P. Coppens, L. Li, and N. J. Zhu, Journal of the American Chemical Society **105**, 6173 (1983).
[15] M.-S. Liao and S. Scheiner, The Journal of Chemical Physics **114**, 9780 (2001).
[16] T. Kroll, R. Kraus, R. Schönfelder, V. Y. Aristov, O. V. Molodtsova, P. Hoffmann, and M. Knupfer, The Journal of Chemical Physics **137**, 054306 (2012).
[17] N. Marom and L. Kronik, Applied Physics A **95**, 165 (2009).
[18] K. Nakamura, Y. Kitaoka, T. Akiyama, T. Ito, M. Weinert, and A. J. Freeman, Physical Review B **85**, 235129 (2012).
[19] S. Stepanow, P. S. Miedema, A. Mugarza, G. Ceballos, P. Moras, J. C. Cezar, C. Carbone, F. M. F. de Groot,

and P. Gambardella, Physical Review B **83**, 220401 (2011).
[20] P. S. Miedema, S. Stepanow, P. Gambardella, and F. M. F. d. Groot, Journal of Physics: Conference Series **190**, 012143 (2009).
[21] M. D. Kuzmin, A. Savoyant, and R. Hayn, The Journal of Chemical Physics **138**, 244308 (2013).
[22] D. J. Newman and B. Ng, Reports on Progress in Physics **52**, 699 (1989).
[23] P. A. Reynolds and B. N. Figgis, Inorganic Chemistry **30**, 2294 (1991).
[24] B. Thole, G. Van Der Laan, and P. Butler, Chemical Physics Letters **149**, 295 (1988).
[25] G. Filoti, M. Kuz'min, and J. Bartolomé, Physical Review B **74** (2006).
[26] J. Bartolomé, F. Bartolomé, L. M. García, G. Filoti, T. Gredig, C. N. Colesniuc, I. K. Schuller, and J. C. Cezar, Physical Review B **81**, 195405 (2010).
[27] J. Fernández-Rodríguez, B. Toby, and M. van Veenendaal, Journal of Electron Spectroscopy and Related Phenomena **202**, 81 (2015).
[28] `https://subversion.xray.aps.anl.gov/xclaim/xclaim.html`.
[29] B. T. Thole, P. Carra, F. Sette, and G. van der Laan, Phys. Rev. Lett. **68**, 1943 (1992).
[30] P. Carra, B. T. Thole, M. Altarelli, and X. Wang, Physical Review Letters **70**, 694 (1993).
[31] R. Cowan, *The Theory of Atomic Structure and Spectra* (1981).
[32] `http://www.tcd.ie/Physics/People/Cormac.McGuinness/Cowan/`.
[33] J. Mulak and Z. Gajek, *The effective crystal field potential* (2000).
[34] M. W. Haverkort, *Spin and orbital degrees of freedom in transition metal oxides and oxide thin films studied by soft x-ray absorption spectroscopy, Ph.D. Thesis* (2005), URL `http://kups.ub.uni-koeln.de/1455/`.
[35] D. A. Varshalovich, A. N. Moskalev, and V. K. Khersonskii, *Quantum Theory of Angular Momentum* (1988).
[36] J. Fuggle and J. Inglesfield, *Unoccupied Electronic States* (1992).
[37] J. Stöhr and H. König, Physical Review Letters **75**, 3748 (1995).
[38] T. Oguchi and T. Shishidou, Physical Review B **70**, 024412 (2004).
[39] J. P. Crocombette, B. T. Thole, and F. Jollet, Journal of Physics: Condensed Matter **8**, 4095 (1996).
[40] C. Piamonteze, P. Miedema, and F. de Groot, Physical Review B **80**, 184410 (2009).
[41] C. T. Chen, Y. U. Idzerda, H.-J. Lin, N. V. Smith, G. Meigs, E. Chaban, G. H. Ho, E. Pellegrin, and F. Sette, Phys. Rev. Lett. **75**, 152 (1995).
[42] P. Bruno, Physical Review B **39**, 865 (1989).
[43] G. v. d. Laan, Journal of Physics: Condensed Matter **10**, 3239 (1998).
[44] M. Kuz'min, R. Hayn, and V. Oison, Physical Review B **79**, 024413 (2009).
[45] C. Wäckerlin, K. Tarafder, D. Siewert, J. Girovsky, T. Hhlen, C. Iacovita, A. Kleibert, F. Nolting, T. A. Jung, P. M. Oppeneer, et al., Chemical Science **3**, 3154 (2012).
[46] W. Harrison, *Electronic Structure and the Properties of Solids* (1980).
[47] S. Bhandary, S. Ghosh, H. Herper, H. Wende, O. Eriksson, and B. Sanyal, Physical Review Letters **107** (2011).
[48] Y. Tsujimoto, C. Tassel, N. Hayashi, T. Watanabe, H. Kageyama, K. Yoshimura, M. Takano, M. Ceretti, C. Ritter, and W. Paulus, Nature **450**, 1062 (2007), ISSN 1476-4687.
[49] J. M. Pruneda, J. iguez, E. Canadell, H. Kageyama, and M. Takano, Phys. Rev. B **78**, 115101 (2008).
[50] In D_{4h} the labeling ^3E_g can correspond to different ground states. We denote the configurations $(a_{1g}^1 e_g^3 b_{2g}^2)$ and $(a_{1g}^2 e_g^3 b_{2g}^1)$ as $^3E_g(a)$ and $^3E_g(b)$ respectively.